

Quantum Monte Carlo Study of High Pressure Solid Molecular Hydrogen

Sam Azadi¹, W. M. C. Foulkes¹, Thomas D. Kühne²

¹ Thomas Young Centre and Department of Physics, Imperial College London, London SW7 2AZ, United Kingdom

² Institute of Physical Chemistry and Centre for Computational Sciences, Johannes Gutenberg University Mainz, Staudinger Weg 9, 55128 Mainz, Germany

E-mail: s.azadi@imperial.ac.uk

Abstract. We use the diffusion quantum Monte Carlo (DMC) method to calculate the ground state phase diagram of solid molecular hydrogen and examine the stability of the most important insulating phases relative to metallic crystalline molecular hydrogen. We develop a new method to account for finite-size errors by combining the use of twist-averaged boundary conditions with corrections obtained using the Kwee-Zhang-Krakauer (KZK) functional in density functional theory. To study band-gap closure and find the metallization pressure, we perform accurate quasi-particle many-body calculations using the *GW* method. In the static approximation, our DMC simulations indicate a transition from the insulating Cmca-12 structure to the metallic Cmca structure at around 375 GPa. The *GW* band gap of Cmca-12 closes at roughly the same pressure. In the dynamic DMC phase diagram, which includes the effects of zero-point energy, the Cmca-12 structure remains stable up to 430 GPa, well above the pressure at which the *GW* band gap closes. Our results predict that the semimetallic state observed experimentally at around 360 GPa [Phys. Rev. Lett. **108**, 146402 (2012)] may correspond to the Cmca-12 structure near the pressure at which the band gap closes. The dynamic DMC phase diagram indicates that the hexagonal close packed $P6_3/m$ structure, which has the largest band gap of the insulating structures considered, is stable up to 220 GPa. This is consistent with recent X-ray data taken at pressures up to 183 GPa [Phys. Rev. B **82**, 060101(R) (2010)], which also reported a hexagonal close packed arrangement of hydrogen molecules.

1. Introduction

Solid molecular hydrogen is the simplest and most fundamental quantum molecular crystal. At high pressure it is predicted to become not only a metallic atomic solid [1] but also a high- T_c superconductor [2] and perhaps a superfluid [3]. Although there are experimental results for the structure and phase diagram of high-pressure hydrogen at room temperature, [4, 5, 6, 7, 8] the crystal structures appearing in the complex low-temperature high-pressure phase diagram are not yet completely determined. Spectroscopic investigations using infra-red (IR) and Raman methods suggest the existence of three phases [9]. Phase I, which is stable up to 110 GPa, is a molecular solid composed of quantum rotors arranged in a hexagonal-close-packed (hcp) structure. Changes in the low-frequency regions of the Raman and IR spectra imply the existence of a second phase above 110 GPa; this is known as phase II, or the broken symmetry phase. The continuous behavior of the Raman vibron frequency across the I to II transition suggests that phase II may consist of an arrangement of molecules on an hcp lattice, as in the $P6_3/m$ structure. Calculations based on density functional theory (DFT) predict orthorhombic $Cmc2_1$, $Pca2_1$, and $P2_1/c$ structures [10, 11, 12]. The molecular centres in these structures lie close to those of an hcp lattice, but are incompatible with neutron data for solid deuterium [13]. The appearance of phase III at 150 GPa is accompanied by a large discontinuity in the Raman spectrum and a strong rise in the spectral weight of the IR molecular vibrons. Although the structures of phase II and phase III are not known for certain, recent X-ray results [14] at pressures up to 183 GPa suggest that the hydrogen molecules in both phases lie close to the points of an hcp lattice. Recent infrared and optical absorption results [15] indicate that the molecular structure of phase III persists up to 360 GPa, with no evidence of the onset of a metallic state.

Computational methods used to investigate the high-pressure low-temperature phase diagram of solid molecular hydrogen include density functional theory [12, 16, 11, 17, 18, 19, 20] and quantum Monte Carlo (QMC) [21, 22]. Approaches used to explore the phase space of possible structures include the evolutionary method of Oganov and Glass [23] and the static ab-initio structure searching method of Pickard and Needs, [24] which has also been employed to determine the ground-state structure of *atomic* metallic hydrogen [25]. Recently, a series of four papers [26, 27] presented a fresh look at the high-pressure hydrogen problem. By studying the equalization of the intra- and inter-molecular H-H bond lengths in dense hydrogen, these papers investigated the four most stable structures found by Pickard and Needs [24] using DFT in the static approximation (i.e., ignoring the zero-point vibrational energy of the H atoms).

However, all of the recent calculations of the metallization pressure and phase diagram are based on the single-particle mean-field-like DFT method. This has various drawbacks, such as the band-gap problem and the sensitivity of the results to the choice of exchange-correlation (XC) functional, which affects both the relative stabilities of different phases and the predicted metallization pressure [28]. Furthermore, attempts

to explore the phase space of possible structures have been based primarily on DFT in the static approximation, which ignores the proton zero-point energy (ZPE). Since the ZPE is normally larger than the energy differences between various candidate structures, structure-searching methods including an approximate ZPE should be considered. Most of the existing DFT calculations of solid hydrogen have used the local density approximation (LDA) or the generalized gradient approximation (GGA) to the unknown exchange-correlation functional. Neither of these functionals adequately describes van der Waals (vdW) interactions.

In this paper, we use QMC simulations to determine the ground-state phase diagram of solid molecular hydrogen in the pressure range $100 < P < 400$ GPa. We study, systematically and accurately, the two main factors affecting the quality of the calculated phase diagram: finite-size errors and proton zero-point energy. To investigate the mechanism of metallization and determine the pressure at which the band gap closes, we also carry out many-body perturbation theory calculations within the *GW* approximation. We focus on four specific structures, with space groups $P6_3/m$, $C2/c$, $Cmca-12$, and $Cmca$. According to ground-state static DFT calculations using the Perdew-Burke-Ernzerhof (PBE) version of the generalized gradient approximation [29] (GGA), these are stable in the pressure ranges <105 , 105 – 270 , 270 – 385 , and 385 – 490 GPa, respectively [24].

2. Computational Details

The fixed-node diffusion quantum Monte Carlo (DMC) algorithm [30] yields the energy expectation value of the variationally optimal wave function with the same nodal surface (surface of zeros) as a chosen many-electron trial function. The method has a long history and has been thoroughly benchmarked [30]. For small molecules, where almost exact results can be obtained using quantum chemical methods, ground-state total energies calculated using fixed-node DMC are consistently more accurate than energies calculated DFT, typically by a factor of 10 or more. Unlike DFT, fixed-node DMC also provides a good description of the dependence of the total energy on coordination number (very important when comparing the energies of different crystal structures) and a fairly good description of the potential surface during bond-breaking processes. For large systems such as the ones studied in this paper, fixed-node DMC is the most accurate known ground-state total energy method and the only possible benchmarks are against experiment. Again, however, DMC consistently outperforms DFT. For example, the measured cohesive energy of crystalline Si is 4.62 eV/atom; fixed-node DMC simulations yields 4.63 eV/atom [31]; and DFT in the local spin-density approximation yields 5.28 eV/atom. In this unusually favorable case, the DMC result is 65 times more accurate than the DFT result. The ability of DMC to describe changes in coordination is illustrated by the example of the Si self-interstitial defect [31]. The DMC value of the defect formation energy, which is in good agreement with experiment, is about 1 eV larger than the PW91 GGA value and 1.5 eV larger than the

LDA values. The main drawback of DMC, which explains why it is not more widely used, is the computational cost: a DMC simulation typically costs about 10^4 times more than a DFT simulation of the same system.

DMC can also be used to obtain limited information about excited states. However, other approaches such as the *GW* method used in this work are generally better for excitation spectra. The results of *GW* calculations of the band gaps of *sp*-bonded materials generally match experiment to within a few tenths of an eV.

Our fixed-node DMC simulations used the CASINO QMC code [32] and a trial function of Slater-Jastrow (SJ) form,

$$\Psi_{SJ}(\mathbf{R}) = \exp[J(\mathbf{R})] \det[\psi_n(\mathbf{r}_i^\uparrow)] \det[\psi_n(\mathbf{r}_j^\downarrow)],$$

where \mathbf{R} is a $3N$ -dimensional vector that defines the positions of all N electrons, \mathbf{r}_i^\uparrow is the position of the i 'th spin-up electron, \mathbf{r}_j^\downarrow is the position of the j 'th spin-down electron, $\exp[J(\mathbf{R})]$ is the Jastrow factor, and $\det[\psi_n(\mathbf{r}_i^\uparrow)]$ and $\det[\psi_n(\mathbf{r}_j^\downarrow)]$ are Slater determinants of spin-up and spin-down one-electron orbitals. These orbitals were obtained from DFT calculations using the plane-wave-based Quantum Espresso code [33]. A norm-conserving pseudopotential constructed within DFT using the PBE exchange-correlation functional was employed. [34] Previous work has shown that the pseudopotential approximation has a very small impact on the results of calculations of high-pressure solid hydrogen [25]. We chose a very large basis-set cut-off of 300 Ry to guarantee converge to the complete basis set limit [35]. The plane-wave orbitals were transformed into a blip polynomial basis [36]. Our Jastrow factor consists of polynomial one-body electron-nucleus (en) and two-body electron-electron (ee) terms, the parameters of which were optimized by variance minimization at the variational Monte Carlo (VMC) level [37, 38].

Geometry and cell optimizations were carried out using DFT with a dense $16 \times 16 \times 16$ \mathbf{k} -point mesh. The BFGS quasi-Newton algorithm, as implemented in the Quantum Espresso package, was used for both cell and geometry optimization, with convergence thresholds on the total energy and forces of 0.01 mRy and 0.1 mRy/Bohr, respectively, to guarantee convergence of the total energy to less than 1 meV/proton and the pressure to better than 0.1 GPa. An investigation of the proton-proton distance of accurately relaxed structures in the pressure range of 100-450 GPa reveals two main features. First, as the pressure increases, the intra-molecular H_2 bond length (nearest-neighbor distance) increases slightly, rising from 0.735 Å to 0.778 Å. This could be a consequence of a weakening of the H_2 bonds as the coordination of the H atoms increases. Second, unlike the intra-molecular H_2 bond length, the inter-molecular distance decreases smoothly as the pressure rises. Details of the behavior of the inter-atomic distance with pressure and of the experimental evidence are presented in Ref [26].

Table 1. VMC and DMC energies of the P6₃/m phase calculated using PBE and PBE0 single-particle orbitals. Energies and pressures are in eV per proton and GPa, respectively.

Pressure	PBE-VMC	PBE0-VMC	PBE-DMC	PBE0-DMC
100	-15.1335(4)	-15.1397(4)	-15.2327(3)	-15.2338(3)
200	-14.5898(4)	-14.5979(4)	-14.6856(3)	-14.6867(3)
300	-14.0473(4)	-14.0524(4)	-14.2184(3)	-14.2193(3)

3. Results and discussion

3.1. Effect of single-particle Slater determinant on QMC energy

Our recent DFT work [20] showed that hybrid exchange-correlation functionals including a small fraction of exact exchange favor insulating phases relative to metallic phases. We therefore investigate how the choice of density functional used to calculate the one-electron orbitals appearing in the Slater determinants (and thus to define the fixed nodal surface) affects our QMC results. For this purpose, we compared the VMC and DMC energies of the insulating P6₃/m phase (which has the largest band gap of the four structures considered) using orbitals calculated using the semi-local PBE GGA functional [29] and the PBE0 hybrid functional including 25% exact exchange [39]. The VMC and DMC calculations were performed at the Γ point of the Brillouin zone of a simulation cell containing 128 hydrogen atoms and $2 \times 2 \times 2$ replicas of the P6₃/m unit cell. The VMC and DMC energies at pressures 100 GPa, 200 GPa and 300 GPa, are given in Table 1.

The difference between the PBE and PBE0 energies is about 6 meV/atom at the VMC level and 1 meV/atom at the DMC level. Similar calculations for the Cmca-12 structure at two different pressures gave similar results. This demonstrates that, in the case of solid molecular hydrogen, DMC energies calculated using PBE and PBE0 orbitals differ negligibly, even though the change of functional has a large effect on the DFT phase diagram [20]. The very weak dependence of the DMC energy on the choice of single-particle orbitals suggests, furthermore, that the fixed-node errors are small. This contrasts with the case of 3d transition metal compounds [40], where changing the DFT exchange-correlation functional does affect the DMC results.

3.2. Finite-size correction to the DMC energy

When simulating infinite periodic systems or finite systems subject to periodic boundary conditions, it is not possible to use the familiar $1/r$ form of the Coulomb interaction because the sums over images of the simulation cell do not converge absolutely. The standard solution to this problem is to replace the Coulomb interaction by the Ewald interaction. The three-dimensional Ewald interaction is the periodic solution of Poisson's equation for a periodic array of point charges embedded in a uniform

Table 2. DMC energies of the Cmca phase at $P = 300$ GPa for different number N of particles in simulation cell, N . FS corrections obtained using combination of TABC and DFT-based KZK functional has been applied to the DMC results. Energies are in eV per proton.

N	DMC-TABC
64	-14.1829(6)
96	-14.1931(3)
128	-14.1936(3)
144	-14.1927(4)

neutralizing background and is therefore appropriate for an electrically unpolarized, neutral system [41]. All DMC results reported in this paper were calculated using the Ewald [42] electron-electron interaction.

In DFT, the limit of infinite system size can be approached by improving the \mathbf{k} -point sampling, but QMC calculations have to be performed using increasingly large simulation cells. The resulting finite-size (FS) effects are a significant source of error. The following QMC results used C2/c, Cmca-12, P6₃/m and Cmca simulation cells containing 96, 96, 128, and 144 atoms, respectively, equivalent to $2 \times 2 \times 2$, $2 \times 2 \times 2$, $2 \times 2 \times 2$ and $3 \times 2 \times 3$ repetitions of the corresponding unit cells. QMC FS errors are conventionally separated into one-body and two-body contributions. One-body (independent-particle) errors arise from the non-interacting kinetic, potential and Hartree energies; two-body errors arise from the effects of exchange and correlation on the Coulomb and kinetic energies.

This work accounts for FS errors by correctly and accurately combining the use of twist-averaged boundary conditions (TABC) [43] with DFT-based corrections obtained using the size-dependent Kwee-Zhang-Krakauer (KZK) functional [44]. By construction, KZK corrections remove the finite-size errors in DMC calculations of cubic homogeneous systems exactly; our systems are neither cubic nor homogeneous, but we show below that the KZK approach still works remarkably well. Our DMC-TABC energies were averages over 12 random twists, corresponding to 12 randomly translated Monkhorst-Pack \mathbf{k} -point meshes. The KZK correction is given by $FS^{KZK} = E^{LDA}(\infty) - E^{KZK}(L)$, where $E^{LDA}(\infty)$ is the DFT energy computed within the local density approximation (LDA) using a fully converged \mathbf{k} -point mesh (which in this work means $24 \times 24 \times 24$), and $E^{KZK}(L)$ is obtained from DFT-KZK calculations employing the same simulation cell and twists as our DMC-TABC results. In the case of the metallic Cmca structure, we also carried out DMC-TABC calculations using 24 twists; the change in the total energy was about 1.4 meV/proton at $P = 400$ GPa, implying that DMC energies obtained by combining TABC and KZK FS-corrections converge very rapidly as the number of twists is increased.

To check the accuracy and convergence of the DMC energy as a function of the number of protons N in the simulation cell, we performed calculations for different N .

Table 2 shows the results for the metallic Cmca phase at $P = 300$ GPa. The convergence of the TABC-DMC energy with increasing N is excellent and there is no difficulty in reaching the accuracy of 1 meV per proton necessary for high-pressure hydrogen phase diagram calculations. We emphasize the importance of our approach to the treatment of finite-size errors as an application of TABC to real systems [45].

3.3. Metallization pressure

To find the metallization pressure, quasi-particle band gaps were calculated within the GW approximation using the Yambo code [46]. Non-self-consistent GW calculations were performed starting from DFT wave functions, using a plasmon pole approximation for the dielectric function [47, 48]. Following convergence checks, the numbers of unoccupied bands and \mathbf{k} -points were set to 200 and 512, respectively. We also checked convergence with respect to the number of plane waves, which was set to 1800 for the $P6_3/m$ structure and 2700 for the Cmca-12 and C2/c structures. It is important to point out that our GW and DMC results are independent of one another. DMC is used to calculate the enthalpy as a function of pressure, whilst GW is used to calculate the quasi-particle band gap as a function of pressure. Both methods use the same relaxed DFT crystal structures, but they are otherwise unrelated.

In the following, we present the metallization pressure of the Cmca-12 phase as obtained using the PBE, PBE0, and GW approximations. We use the simplest estimate of the metallization pressure, which is the pressure at which the energy band gap closes. To estimate the metallization pressure from the calculated band gaps at a few different pressures, we linearly extrapolate the band gap as a function of pressure. Figure 1 illustrates band-gap closure in the Cmca-12 phase. The PBE, PBE0, and GW results show that the band gap of Cmca-12 vanishes at pressures of 245, 309, and 373 GPa, respectively. The PBE metallization pressure is in agreement with the value estimated by Pickard and Needs [24]. From band-structure calculations we see that the Cmca-12 phase has an indirect band gap; the linear decrease of the band gap with pressure is not unexpected in indirect gap structures and is also reported experimentally [9].

As usual, band gaps calculated using the semi-local PBE functional are much too small. A significant contributor to this band-gap underestimation is the inability of *any* analytic functional of the density to represent the discontinuous change in exchange-correlation potential that occurs as a single electron is added to a system with a filled band [49]. By including a fraction of the exact non-local orbital-dependent exchange energy, the PBE0 hybrid functional circumvents this problem to some extent. However, even the PBE0 band gap is considerably smaller than the GW band gap, which is expected to be more accurate.

Our GW results show that the band gaps of the $P6_3/m$, C2/c, and Cmca-12 structures vanish at the static pressures of 446, 398, and 373 GPa, respectively. Semilocal DFT, hybrid-DFT [20], and GW calculations all show that $P6_3/m$ has the largest band gap and, consequently, the largest metallization pressure of the

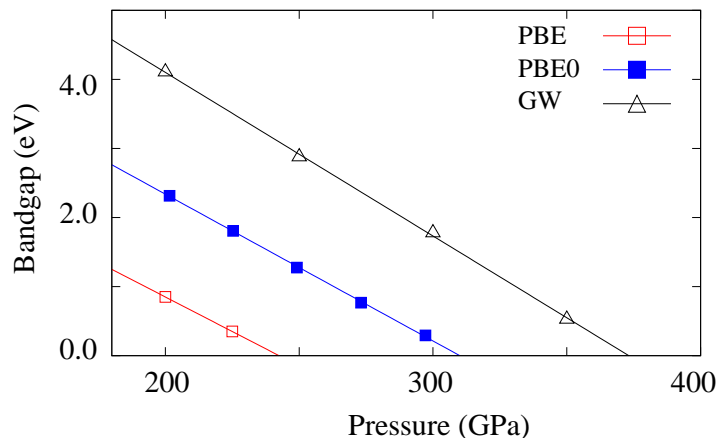


Figure 1. (Color online) Band gap of the Cmca-12 crystal structure as a function of pressure as calculated using the PBE, PBE0, and *GW* approximations.

three insulating structures considered. The *GW* indirect band gap and its pressure dependence agree very well with recently reported experimental results [50].

3.4. Static DMC phase diagram

In the following, we present enthalpy-pressure diagrams obtained from DMC simulations at the static level of theory, which ignores proton ZPE. Figure 2 illustrates H_{stat} as a function of pressure. Within the static approximation, the $P6_3/m$ structure is the most stable up to pressures of approximately 250 GPa, but is less stable than both $C2/c$ and Cmca-12 by 350 GPa. The error bars make it difficult to establish exactly where the transition from $P6_3/m$ to $C2/c$ or Cmca-12 takes place or to say which of $C2/c$ or Cmca-12 is favored. The transition from $C2/c$ or Cmca-12 to the metallic Cmca phase happens around 375 GPa.

Thus, within the static approximation, DMC predicts that the hexagonal close packed $P6_3/m$ structure is more stable than the other structures investigated over the entire pressure range at which phases I and II exist experimentally, and that it remains more stable well above the measured transition to phase III. As already discussed above, recent X-ray results [14] at pressures up to 183 GPa suggest that hcp symmetry is a strong candidate not only for phase II but also for phase III.

We claim that our static DMC phase diagram is much more accurate than the static DFT phase diagram. One reason is the importance of vdW interactions between hydrogen molecules, which significantly influence the phase diagram, especially at low densities. QMC calculations have recently shown that the vdW interaction has a substantial effect on the transition pressures between the crystalline phases of ice at high pressure [52] and one would expect them to matter even more in solid molecular hydrogen. An important consequence is that transition pressures obtained from standard DFT functionals, which neglect vdW forces, are likely to be unreliable. Because of this recognition, some very recent work [53] has used van der Waals density

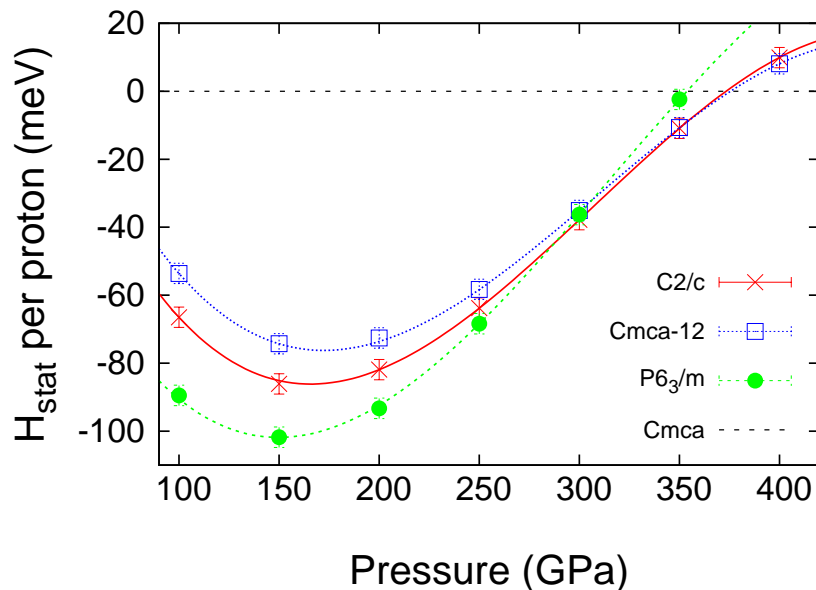


Figure 2. (color online). Enthalpy as a function of pressure calculated using the DMC-TABC method in the static approximation.

functionals to study solid H. There is no need to emphasize that DMC provides a highly accurate description of exchange and correlation in relatively weakly correlated materials and that it includes an excellent quantitative treatment of vdW forces.

Combining our static DMC phase diagram and *GW* results suggests: (a) that the well known rule of thumb “the lower the energy the wider the gap” [51] is valid here; and (b) that metallization occurs via a transition from the zero band-gap Cmca-12 structure to the metallic Cmca structure at around 375 GPa. The agreement between the pressure at which the *GW* band gap of the Cmca-12 structure closes and the pressure at which DMC predicts a phase transition from Cmca-12 to the metallic Cmca structure is remarkable but fortuitous, since including the effects of phonon zero-point energy changes the picture.

3.5. Dynamic DMC phase diagram

The above scenario is based on the static approximation. In reality, even in the ground state, H₂ molecules are quantum oscillators with a natural frequency of $\sim 10^{14}$ Hz (for the H–H bond stretching) and a significant ZPE. Following standard practice in the field, our treatment of ZPE uses the harmonic approximation. A full analysis of anharmonicity is beyond the scope of this paper, but estimating the ZPE within the harmonic approximation is feasible [24] and widely believed to produce accurate results in the case of the molecular solid hydrogen. The harmonic approximation has also been used for atomic metallic hydrogen [25].

To include the effects of ZPE, phonon frequencies were calculated using density functional perturbation theory as implemented in Quantum Espresso [33]. The ZPE per proton was estimated as $E_{ZPE}(V) = 3\hbar\bar{\omega}/2$, where $\bar{\omega} = \sum_{\mathbf{q}} \sum_{i=1}^{N_{mode}} \omega_i(\mathbf{q}) / (N_{\mathbf{q}} N_{mode})$.

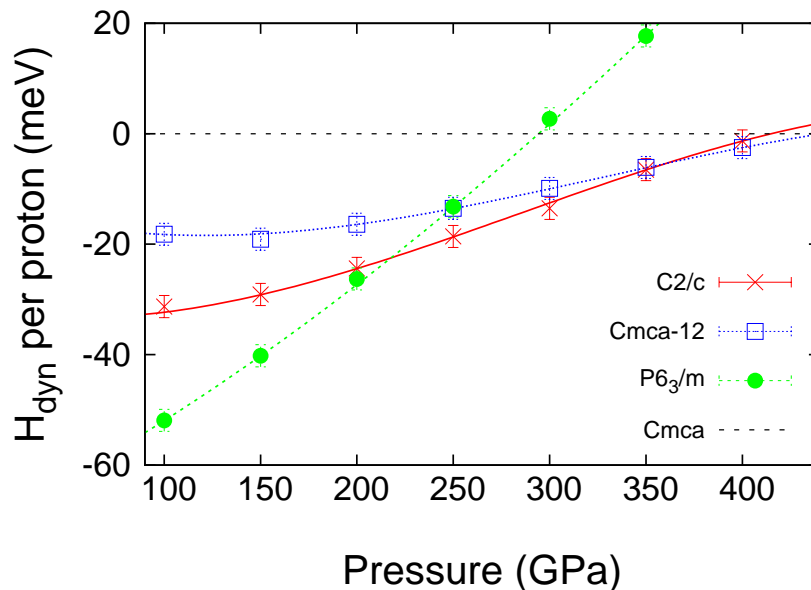


Figure 3. (Color online) Enthalpy as a function of pressure calculated using the DMC-TABC method in the dynamic approximation. The proton ZPE was calculated using DFT.

Here N_{mode} and $N_{\mathbf{q}}$ are the number of vibrational modes in the unit cell and the number of phonon wave vectors \mathbf{q} , respectively, $\omega_i(\mathbf{q})$ is the angular frequency of the phonon in band i with wave vector \mathbf{q} , and the summation over \mathbf{q} includes all \mathbf{k} -points on a $2 \times 2 \times 2$ grid in the Brillouin zone. McMahon [25] demonstrated that a \mathbf{q} -point grid of this density is sufficient to converge ZPE differences between structures to within a few percent.

In agreement with previous DFT results [24], we find that the ZPE is large, structure dependent, and density dependent, ranging from 257 meV per proton at low density to 351 meV per proton at high density. The P6₃/m structure has the largest and the Cmca structure the smallest ZPE over the whole range of pressures considered. The C2/c and Cmca-12 structures have almost the same ZPE, which lies between the P6₃/m and Cmca values.

By defining $H_{dyn} = E_{dyn} + PV$, where $E_{dyn} = E_{stat} + ZPE$, we obtain the dynamic phase diagram of solid molecular hydrogen illustrated in Fig. 3.

Bearing in mind the error bars shown in Fig. 3, we see that P6₃/m is the most stable phase up to a pressure of approximately 220 GPa. This is in good agreement with experimental results [14]. As discussed above, because of the tiny enthalpy difference between the C2/c and Cmca-12 phases, it is difficult to determine their pressure stability ranges accurately. However, we are able to conclude that we expect to observe the following structural transitions with increasing pressure: P6₃/m \rightarrow C2/c \rightarrow Cmca-12 \rightarrow Cmca.

Comparing the static and dynamic results, we see that the proton ZPE has two main effects. First, although the order in which the phases appear with increasing

pressure is unaffected, their enthalpies and regions of stability change. If we were to take an optimistic view and ignore the error bars, we would say that $P6_3/m$, $C2/c$, $Cmca-12$, and $Cmca$ phases are now stable in the pressure ranges <220 GPa, $220-360$ GPa, $360-430$ GPa, and >430 GPa, respectively. As in the static case, however, the error bars make it difficult to discriminate between the $C2/c$ and $Cmca-12$ structures over a wide range of pressures, this time from 300 to approximately 450 GPa. Second, the inclusion of ZPE increases the pressure of the transition to the metallic $Cmca$ phase by 14%, which is close to the 10% increase previously reported [16]. If the band gap is of order 0.5 eV (the vibron energy) or less, which is comparable to the $Cmca-12$ gap in this pressure range, the inclusion of ZPE effects is also expected to increase the gap. [16] The increase is small, however, and the gap still closes before the transition to the $Cmca$ structure takes place. This leaves a region of 20–30 GPa where the $Cmca-12$ phase persists but is no longer insulating. We, also, found that the ZP pressures are quite small and has no significant effect on the phase diagram.

A comparison of the densities of different structures at the same pressure shows that, in phases II and III: $\text{density}(Cmca) > \text{density}(Cmca-12) > \text{density}(C2/c) > \text{density}(P6_3/m)$. As the pressure is increased, the PV term in the enthalpy rises faster for the low-density insulating phases than for the metallic phase, reducing the relative stability of the insulating phases and leading eventually to the metal-insulator transition. The difference between the densities of the insulating phases and the metallic $Cmca$ phase reduces at high pressure, especially in the case of the $Cmca-12$ structure.

The differences between the DMC and DFT phase diagrams are primarily due to the internal energy term in the enthalpy. For pressures up to 220 GPa, the DMC energy of the low density $P6_3/m$ phase lies further below the energies of the other phases, especially the high-density metallic $Cmca$ phase, than does the DFT energy. Our results, at both the static and dynamic levels, predict that the $P6_3/m$ phase is the most stable of the structures considered for a large range of pressures up to 220 GPa in the dynamic case or 280 GPa in the static case. This prediction is consistent with the latest low temperature X-ray powder-diffraction results [14], which indicate that the hydrogen molecules in phases II and III are still in a hexagonal structure and that phase III remains hexagonal up to the maximum experimental pressure of 183 GPa. The nature of the difference between phases II and III remains to be established, but may be related to a classical orientational ordering of the H_2 molecules [54].

4. Conclusion

In conclusion, we have used DMC simulations to study the phase diagram of the four most stable structures of high pressure hydrogen found from DFT calculations. We accurately computed the FS corrections by correctly combining the use of TABC with the DFT-KZK method. We also carried out GW calculations to find the metallization pressure. Our GW results show that the band gap of the insulating $Cmca-12$ phase closes at 373 GPa, whilst our DMC simulations in the dynamic approximation show that the

Cmca-12 structure may remain stable up to 430 GPa, at which point it transforms to the metallic Cmca phase. We propose that the semimetallic state observed experimentally at around 360 GPa [15] may correspond to the Cmca-12 structure near the pressure at which the band gap closes. At high pressures our DMC results are in qualitative agreement with previous DFT calculations [24], and suggest that the metallization of solid molecular hydrogen happens through the transformation of the Cmca-12 phase to the Cmca structure. Our DMC results indicate that the hcp structure $P6_3/m$, which has the lowest density and the largest band gap of the phases considered, is the most stable molecular structure up to 220 GPa.

We acknowledge interesting and helpful discussions with Richard Needs and Chris Pickard.

References

- [1] E. Wigner and H. B. Huntington, *J. Chem. Phys.* **3**, 764 (1935).
- [2] N. W. Ashcroft, *Phys. Rev. Lett.* **21**, 1748 (1968).
- [3] E. Babaev, A. Sudbo, and N. W. Ashcroft, *Nature (London)* **431**, 666 (2004).
- [4] P. Loubeyre, R. LeToullec, D. Hausermann, M. Hanfland, R. J. Hemley, H. K. Mao, and L. W. Finger, *Nature* **383**, 702 (1996).
- [5] P. Loubeyre, F. Occelli, and R. LeToullec, *Nature* **416**, 613 (2002).
- [6] A. F. Goncharov, E. Gregoryanz, R. J. Hemley, and H-K. Mao, *Proc. Natl Acad. Sci.* **98**, 14234 (2001).
- [7] M. I. Erements and I. A. Troyan, *JETP Lett.* **89**, 174 (2009).
- [8] M. I. Erements and I. A. Troyan, *Nature Materials*, **10** 927 (2011).
- [9] H. K. Mao and R. J. Hemley, *Rev. Mod. Phys.* **66**, 671 (1994).
- [10] H. Kitamura, Sh. Tsuneyuki, O. Tadashi, and T. Miyake, *Nature* **404**, 259 (2000).
- [11] J. Kohanoff, S. Scandolo, G. L. Chiarotti, and E. Tosatti, *Phys. Rev. Lett.* **78**, 2783 (1997).
- [12] K. A. Johnson, and N. W. Ashcroft, *Nature* **403**, 632–635 (2000).
- [13] I. Goncharenko, and P. Loubeyre, *Nature* **435**, 1206–1209 (2005).
- [14] Y. Akahama, M. Nishimura, H. Kawamura, N. Hirao, Y. Ohishi, and K. Takemura, *Phys. Rev. B* **82**, 060101(R) (2010).
- [15] C-S Zha, Z. Liu, and R. J. Hemley, *Phys. Rev. Lett.* **108**, 146402 (2012).
- [16] M. Stadele, and R. M. Martin, *Phys. Rev. Lett.* **84**, 6070 (2000).
- [17] J. Kohanoff, S. Scandolo, S. de Gironcoli, and E. Tosatti, *Phys. Rev. Lett.* **83**, 2783 (1999).
- [18] H. Chacham, and S. Louie, *Phys. Rev. Lett.* **66**, 64 (1991).
- [19] K. Nagao, H. Nagara, and S. Matsubara, *Phys. Rev. B* **56**, 2295 (1997).
- [20] Sam Azadi and Thomas D.Kuhne, *JETP Lett.* **95**, 509 (2012).
- [21] V. Natoli, R. M. Martin, and D. Ceperly, *Phys. Rev. Lett.* **74**, 1601 (1995).
- [22] V. Natoli, R. M. Martin, and D. Ceperly, *Phys. Rev. Lett.* **70**, 1952 (1993).
- [23] A. R. Oganov, and C. W. Glass. *J. Chem. Phys.* **124**, 244704 (2006).
- [24] C. J. Pickard, and R. J. Needs, *Nature* **3**, 473 (2007).
- [25] J. M. McMahon, and D. M. Ceperley, *Phys. Rev. Lett.* **106**, 165302 (2011).
- [26] V. Labet, P. Gonzalez-Morelos, R. Hoffmann, and N. W. Ashcroft. *J. Chem. Phys.* **136** 074501 (2012).
- [27] V. Labet, R. Hoffmann, and N. W. Ashcroft. *J. Chem. Phys.* **136** 074502, 074503, 074504 (2012).
- [28] S. Azadi and W. M. C. Foulkes, *Phys. Rev. B* (accepted for publication) (2013).
- [29] J. P. Perdew, K. Burke, and M. Ernzerhof, *Phys. Rev. Lett.* **77**, 3865 (1996).
- [30] W. M. C. Foulkes, L. Mitas, R. J. Needs, and G. Rajagopal, *Rev. Mod. Phys.* **73**, 33 (2001).
- [31] W.-K. Leung, R. J. Needs, G. Rajagopal, S. Itoh, and S. Ihara, *Phys. Rev. Lett.* **83**, 2351 (1999).

- [32] R. J. Needs, M. D. Towler, N. D. Drummond, and P. Lopez Rios, *J. Phys.:Condens. Matter* **22**, 023201 (2010).
- [33] P. Giannozzi et al., *J. Phys.: Condens. Matt.* **21**, 395502 (2009).
- [34] P.H.L Sit, and N. Marzari, *J. Chem. Phys.* **122**, 204510 (2005).
- [35] S. Azadi, C. Cavazzoni, and S. Sorella, *Phys. Rev. B* **82**, 125112 (2010).
- [36] D. Alfè and M. J. Gillan, *Phys. Rev. B* **70**, 161101(R) (2004).
- [37] C. J. Umrigar, K. G. Wilson, and J. W. Wilkins, *Phys. Rev. Lett.* **60**, 1719 (1988).
- [38] N. D. Drummond and R. J. Needs, *Phys. Rev. B* **72**, 085124 (2005).
- [39] C. Adamo and V. Barone, *J. Chem. Phys.* **110**, 6158 (1999).
- [40] J. Kolorenc, S. Hu, and L. Mitas, *Phys. Rev. B* **82**, 115108 (2010).
- [41] P. P. Ewald, *Ann. Phys.* **64**, 253 (1921).
- [42] N. D. Drummond, R. J. Needs, A. Sorouri, and W. M. C. Foulkes, *Phys. Rev. B* **78**, 125106 (2008).
- [43] C. Lin, F. H. Zong, and D. M. Ceperley, *Phys. Rev. E* **64** 016702 (2001).
- [44] H. Kwee, S. Zhang, and H. Krakauer, *Phys. Rev. Lett.* **100**, 126404 (2008).
- [45] S. Azadi and W. M. C. Foulkes (to be published).
- [46] A. Marini, C. Hogan, M. Gruning and D. Varsano, *Comput. Phys. Commun.* **180**,1392 (2009).
- [47] L. Hedin, *Phys. Rev.* **139**, A796 (1965).
- [48] M. Gruning, A. Marini, and A. Rubio, *J. Chem. Phys.* **124**, 154108 (2006)
- [49] L. J. Sham, and M. Schlüter, *Phys. Rev. Lett.* **51**, 1888 (1983), J. P. Perdew, and M. Levy, *Phys. Rev. Lett.* **51**, 1884 (1983).
- [50] A. F. Goncharov, J. S. Tse, H. Wang, J. Yang, V. V. Struzhkin, R. T. Howie, and E. Gregoryanz, *Phys. Rev. B* **87**, 024101 (2013).
- [51] E. Kaxiras, J. Broughton, and R. J. Hemley, *Phys. Rev. Lett.* **67**, 1138 (1991).
- [52] B. Santra, J. Klimes, D. Alfe, A. Tkatchenko, B. Slater, A. Michaelides, R. Car, and M. Scheffler, *Phys. Rev. Lett.* **107**, 185701 (2011).
- [53] M. A. Morales, J. M. McMahon, C. Pierleoni, and D. M. Ceperley, *Phys. Rev. Lett.* **110**, 065702 (2013).
- [54] I. I. Mazin, Russell J. Hemley, A. F. Goncharov, Michael Hanfland, and Ho-kwang Mao, *Phys. Rev. Lett.* **78**, 1066 (1997).